Identification of simultaneous U(VI) sorption complexes and U(IV) nanoprecipitates on the magnetite (111) surface

David M. Singer[*1,2], *Shawn M. Chatman*[3], *Eugene S. Ilton*[3], *Kevin M. Rosso*[3], *Jillian F. Banfield*[1], *and Glenn A. Waychunas*[2]

1. Department Earth & Planetary Sciences, University of California, Berkeley

2. Earth Sciences Division, Lawrence Berkeley National Laboratory

3. Fundamental and Computational Sciences Directorate, Pacific Northwest National Laboratory

*Corresponding author: dmsinger@lbl.gov

ABSTRACT

Sequestration of uranium (U) by magnetite is a potentially important sink for U in natural and contaminated environments. However, molecular-scale controls which favor U(VI) uptake including both adsorption of U(VI) and reduction to U(IV) by magnetite remain poorly understood, in particular the role of U(VI)-CO_3-Ca complexes in inhibiting U(VI) reduction. To investigate U uptake pathways on magnetite as a function of U(VI) aqueous speciation, we performed batch sorption experiments on (111) surfaces of natural single crystals under a range of solution conditions (pH 5 and 10; 0.1 mM U(VI); 1 mM $NaNO_3$; and with or without 0.5 mM CO_3 and 0.1 mM Ca) and characterized surface-associated U using grazing incidence extended x-ray absorption fine structure spectroscopy (GI-EXAFS), grazing incidence x-ray diffraction (GI-XRD), and scanning electron microscopy (SEM). In the absence of both carbonate ($[CO_3]_T$, denoted here as CO_3) and calcium (Ca), or in the presence of CO_3 only, co-existing adsorption of U(VI) surface species and reduction to U(IV) occurs at both pH 5 and 10. In the presence of both Ca and CO_3, only U(VI) adsorption (VI) occurs. When U reduction occurs, nanoparticulate UO_2 forms only within and adjacent to surface microtopographic features such as crystal boundaries and cracks. This result suggests that U reduction is limited to defect-rich surface regions. Further, at both pH 5 and 10 in the presence of both CO_3 and Ca, U(VI)-CO_3-Ca ternary surface species develop and U reduction is inhibited. These findings extend the range of conditions under which U(VI)-CO_3-Ca complexes inhibit U reduction.

INTRODUCTION

Uranium (U) has been released into the environment through mining operations, nuclear testing, and accidental spills, and is a contaminant in soils, sediments and groundwater at 70% of the U.S. Department of Energy (DOE) facilities.[1] Development of accurate predictive models of subsurface U transport in such contaminated environments is dependent upon an understanding of the fundamental processes by which U can be sequestered, including adsorption, precipitation, and reduction. Uptake of U by magnetite is a potentially complex process as at least three sequestration pathways are feasible; (1) U(VI) surface adsorption at Fe(II) and/or Fe(III) sites; (2) U(VI) surface adsorption on and/or coprecipitation with Fe(III)-(oxy)hydroxides formed by the weathering and oxidation of Fe(II) from the magnetite; and (3) heterogeneous reduction of U(VI) to U(IV) by Fe(II) at the magnetite surface and the resulting precipitation of an insoluble U(IV)-bearing solid, typically uraninite (UO_2) in the absence of complexing ligands.[2]

Magnetite is a commonly occurring Fe-oxide in the environment, and forms in sediments and soils that are relevant to natural and contaminated settings. In addition, magnetite is used as a sorbent in soil and water remediation.[3, 4] Magnetite has the potential to act as a sink for redox-active metal contaminants in a variety of settings, including contaminated vadose zone sediments [5], and during the corrosion of nuclear waste-bearing steel canisters.[6] The ability of magnetite to effectively reduce aqueous metal species has been shown for a variety of contaminants, including arsenic(V) [7], chromium(VI) [8, 9], and mercury(II).[10] A fundamental understanding of these heterogeneous redox processes is required for developing predictive models for contaminant transport in environments that contain Fe(II)-bearing solid phases. However, even in the case of U, there is no consensus regarding the conditions under which U(VI) reduction by magnetite is

favorable, with variable results ranging from complete reduction of U(VI) to U(IV) resulting in the formation of UO_2[6, 11-13], to incomplete reduction.[14-16] Some of these later studies reported the formation of a presumed mixed-valent phase (e.g. ~ U_3O_8) [15] and a U(V)-U(VI) phase with no U(IV).[16] Whereas there is evidence that variable bulk stoichiometry influences redox reactions involving magnetite[17], other factors such as surface composition and defect structure densities, as well as the interplay between U(VI) solution and surface speciation have not been well constrained.

In the current work, our aim was to use a thoroughly characterized magnetite substrate with respect to surface structure and composition, and examine U uptake by magnetite as a function of U aqueous speciation. With respect to the role of aqueous speciation, reduction of uranyl to UO_2 by structural Fe(II) in chlorite is inhibited in the presence of U(VI)-CO_3-Ca aqueous complexes.[18] These results parallel those for biological reduction of U(VI), in which bacteria use U(VI) as a terminal electron acceptor in anaerobic respiration.[19] In these systems, bacteria can reduce U(VI) when in the form of U(VI)-hydrolysis products and U(VI)-CO_3 aqueous complexes, but the presence of Ca inhibits U(VI) reduction.[20-22] Results such as these have provided important insights into the conditions that stabilize U(VI). However, it not clear if this effect is solely due to the formation of aqueous U(VI)-CO_3-Ca complexes which simply lower the total chemical potential of U(VI) in the system, or whether U(VI)-CO_3-Ca complexes also form at the surface of the solid phase. Part of this uncertainty stems from the fact that direct spectroscopic evidence for possible U(VI)-CO_3-Ca surface complexes is difficult to acquire using standard XAS methods. Consequently, the presence or absence of surface bound U(VI)-CO_3-Ca complexes is an open question. If present, a pressing question would be how the U(VI) coordination environment might impact U(VI) reducibility.

Here we focus on the following questions: (1) Does magnetite (111) surface heterogeneity impact U(VI) reduction? (2) What is/are the dominant U sorption product(s)? (3) What are the structures and stoichiometries of U(VI) surface complexes in the presence of CO_3 and Ca and how does Ca limit U(VI) reduction? To answer these questions, we used a combination of benchtop batch sorption experiments, scanning electron microscopy, and synchrotron-based grazing-incidence x-ray absorption spectroscopy (GI-XAS). GI-XAS experiments yield similar metal coordination environment information as bulk XAS, but with greater sensitivity to small amounts of a surface phase [23], and are ideally suited for obtaining chemical information of surface and near-surface phases including U-bearing sorption complexes and surface precipitates.[24, 25] Single crystal experiments allow for a controlled model system where the surface is well defined, and the nature of surface complexes can be studied in great detail.[23] Further, the magnetite (111) surface was chosen because it is the most common magnetite growth face.[26]

MATERIALS AND METHODS

Magnetite preparation and characterization Magnetite crystals used in the present study were prepared from two samples with cubic (100) habit from Balmat, New York, U.S.A. Magnetite crystals from this location are relatively pure; Zn is the highest impurity at ≤ 0.01 wt% and no other significant trace-level impurities.[27] Oriented (111) slabs, approximately 10 mm x 10 mm x 1 mm, were prepared by Princeton Scientific Corp. The desired surface orientation was confirmed by Laue x-ray diffraction to be within 0.05°. The magnetite (111) surface final polishing step was performed in a Coy Laboratories, Inc. anoxic chamber (2% H_2/98% N_2, < 0.1

ppm O_2) using a modified chemical mechanical polishing (CMP) procedure.[26] Detailed information can be found in the *Supporting Information* (SI); briefly, samples are polished with alkaline silica solutions, following by cleaning solutions to remove residual polishing fluids and airborne-deposited surface impurities including adventitious carbon. Surface roughness and stoichiometry after the CMP procedure were determined by contact-mode atomic force microscopy (AFM) and x-ray photoelectron spectroscopy (XPS), respectively (SI). All crystals exhibit topographically negative linear surface features consistent with CMP-based preferential exposure of structurally defective boundaries and, to a lesser extent, cracks and scratches (SI Fig. 1). The domain boundaries are consistent with magnetic closure domain structures observed on magnetite crystals[28-30], and are likely the result of sub-grain domain boundaries within a mosaic single crystal. Closure domains are planar structures that intersect with <111> axes within the magnetite structure to minimize free energy between adjacent internal magnetic domains. They are structurally defective, likely rich in dislocations, and therefore weak with respect to the surrounding domains, and can be typically observed on {110} and {111} surfaces manifesting as regularly repeating linear features. On the (111) surface, we also observed partial "coat hanger" domains (c.f. Özdemir et al., 1995).[29] These features tend to be evenly spaced at 20-50 μm, on the order of several micrometers in length and one to two nanometers in depth, and manifest shallow walls (1-2º). The degree to which the surface structure and stoichiometry on or near these boundaries deviates from the uniform magnetite (111) surface has not been established. Analysis of the AFM images indicates that the post-CMP magnetite (111) samples with a moderate to high density of such surface features (~ 5-10 % surface coverage) have a root mean squared (RMS) roughness of approximately 1.5 ± 0.1 nm. Crystal samples with a low density of surface features (≤ 5 % surface coverage) have an RMS roughness of approximately 0.5 ± 0.1

nm. XPS of post-CMP samples yielded Fe(II)/Fe(total) of 0.27 (± 0.01) (following the methodology in Ilton et al., 2010 [16]), which reflects a mixture of bulk and surface properties, where the oxidation states of bulk stoichiometric magnetite and the top monolayer of the naturally terminated (111) surface have Fe(II)/Fe(total) values of 0.33 and 0.22, respectively.

Batch experiments All experiments were performed in an anaerobic chamber; detailed information regarding the protocol for the batch sorption of U(VI) by magnetite (111) is in the SI. Briefly, magnetite (111) samples were prepared under batch conditions at pH 5 and 10, with varying $[CO_3]_T$ and [Ca] (Table 1). After 12 hrs of exposure to 0.1 mM U(VI)-bearing solutions, the crystals were removed from the solution reservoir, dried rapidly by heating to 90^{o}C for one minute under N_2, and mounted for either SEM or GI-XAS as described below. Changes in the aqueous concentrations of U and Fe were measured by using a Perkin Elmer SCIEX Elan DRC II Inductively Coupled Plasma Mass Spectrometer (ICP-MS).

Scanning electron microscopy Scanning electron microscopy (SEM) analysis was performed at the Environmental Molecular Sciences Laboratory using a field-emission environmental SEM (FEI Model XL30) equipped with an EDX spectrometer (EDAX Model 136-10). The dried samples, see above, were rapidly carbon-coated and transferred to the SEM under N_2. The SEM was run at 15 kV and images were collected in secondary electron mode.

Grazing-incidence x-ray absorption spectroscopy (GI-XAS) and diffraction (GI-XRD) Crystal samples were mounted on an anodized Al platform with a 25 μm Kapton film dome over the sample (SI Fig. 2). Samples were stored for less than 6 hr under N_2 prior to analysis, and the sample cell was purged with He gas (> 99.995%) during data collection. U L_{III}-edge grazing-incidence x-ray absorption near edge structure (GI-XANES) and extended x-ray absorption fine edge structure (GI-EXAFS) spectra were collected at room temperature at beamline 13-IDC at the Advanced Photon Source (APS) using a cryogenically cooled Si (111) double-crystal monochromator.[31] The beam was focused using two Rh-coated Si mirrors in both the vertical and horizontal directions, producing a beam size of (20 μm x 500 μm). A Newport 2+2+kappa-geometry diffractometer was used for sample orientation and mounting. Fluorescence-yield data were collected using a four-element silicon detector (SII NanoTechnology USA Inc.). The angle of the incident x-rays to the crystal surfaces was set to 0.12°, which is less than the critical angle of the substrate over the energy range examined. The x-ray energy was calibrated using an yttrium foil; the first inflection point in the Y K-edge was set to 17038 eV.

The U L_{III}-edge position was set as the half-height of the normalized adsorption edge. The dominant U oxidation state(s) were determined based on the calibrated edge position with respect to uraninite and uranyl nitrate mechanical mixture standards with an uncertainty of the oxidation state of about 5%.[32] Background-subtracted k^3-weighted EXAFS data were analyzed using the SixPACK[33] interface to IFEFFIT.[34] The EXAFS spectra were fit with the linear-combination fitting (LCF) module in SixPACK using the most likely candidates based on the SEM and GI-XANES analyses and several less likely but potentially relevant candidates (i.e., other U-bearing reference or model compounds which are not predicted to occur based on thermodynamic modeling). The reduced chi squared value was used to determine the goodness-

of-fit for the one-, two-, and three-species linear combination fits (SI Table 1). The applications and limitations of linear-combination fitting of EXAFS spectra of complex environmental samples have been described previously.[35] The components used in the LCF were: bulk uraninite[32], nanoparticulate uraninite[32], schoepite[36], boltwoodite[37], and uranyl sorbed on chlorite.[18] The reference sorption samples were reacted under similar solution composition conditions (pH, [U(VI)], $[CO_3]_T$, and [Ca]) as the uranyl-magnetite samples in the current study. Phase-shift and backscattering amplitude functions for quantitative EXAFS fitting were generated using FEFF 7.0[38] from the crystal structures of soddyite[39], liebigite[40], and Fe-substituted phuralumite[41], which have been shown to reliably fit the uranyl oxygen atoms, CO_3/Ca, and Fe nearest neighbors, respectively.

Grazing-incidence x-ray diffraction patterns were collected by keeping the incident x-ray angle set at 0.12^0 and scanning 2θ at a constant energy of 17200 eV. Diffraction patters were collected over the 2θ-range of 5 - 25^0, and a corresponding d-range of 1.6 - 8.1 $Å^{-1}$. Prior to peak identification for reacted samples, diffraction patterns were background-subtracted and normalized using an unreacted magnetite sample.

RESULTS AND DISCUSSION

SEM and EDX analysis of surface particles Observation of magnetite (111) samples exposed to U(VI)-bearing solutions for 12 hours showed nanoparticles form on the surface when CO_3 is both absent and present (Fig. 1 and SI Fig. 3). These roughly spherical particles were approximately 5 nm in diameter, with particle aggregates forming up to 400-500 nm in diameter.

Detailed information regarding particle size analysis has been reported with a parallel kinetic study.[42] These particle clusters were only observed to form in and adjacent to the linear surface features (i.e., crystal domain boundaries and cracks; see Fig. 1D and G and SI Fig. 3A and B). High magnification showed that these particles formed on the slopes of the domain boundaries, as well as forming aggregates bridging across from some of the steeper boundaries and cracks (Fig. 1 E and H). Further, the particle aggregates were never found beyond ~ 500 nm from these surface features.

To ensure that the location and size distribution of these particles was not an artifact of the polishing step in the CMP protocol, two experiments were performed: (1) a subset of polished crystals were not completely washed and therefore remained in contact with colloidal silica (i.e., the polishing solution was allowed to remain on the polished crystal) and (2) properly cleaned crystals were exposed to a high electrolyte concentration that was then allowed to dry in the anaerobic chamber. The experiments were intended to confirm that the topographically negative surface features were not acting as physical traps that preferentially 'collect' particles formed during reaction. In both cases, particles (either colloidal silica or $NaNO_3$ crystals) were observed uniformly over the entire magnetite (111) surface and there was no evidence for preferential deposition and/or precipitation near the surface features. These results suggest that the particles observed at the magnetite (111) surface after reaction with U(VI) represent a site-specific reaction mechanism occurring in and near the surface features.

Under conditions when both Ca and CO_3 were present, no U-bearing particles were observed on the magnetite (111) surface (SI Fig. 3), even though U uptake by the surface did occur (Table 1). The U sorption loading (Γ) was ~ 30 % lower when Ca was present in solution,

at both pH 5 and 10, compared to when Ca was absent. Although it is possible that the formation of U-bearing particles in the absence of Ca was a result of the rapid-drying process prior to carbon-coating via super-saturation of a U(VI)-(hydro-)oxide phases such as schoepite, it is unlikely as it then would have occurred for all cases involving a drying step and would not have displayed the strong apparent correlation between particle location and surface topographic features. Further, the usual morphology of uranyl hydroxides is needle-like or tabular, not roughly spherical.[43]

EDX analysis of these particles indicated the presence of U, Fe, O, and Zn (SI Fig. 4). It is more likely that the EDS spectra represent the overprinting of the signature from a potential U-bearing (hydr-)oxide phase and the magnetite background (O, Fe, and minor Zn), rather than a single phase that contains all elements, given the features of the GI-EXAFS spectra and fit results, discussed below. The lack of a U bearing precipitate in the presence of aqueous Ca indicates that U is likely adsorbed. In contrast when Ca is absent both adsorption and precipitation, likely via reduction to U(IV), is inferred. These observations are consistent with GI-XAS and GI-XRD, as discussed below.

Identification of the dominant U-bearing species Linear-combination fitting (LCF) results of the GI-EXAFS spectra showed that in the absence of Ca at both pH 5 and 10, the sample spectra were best fit by a combination of that for nanoparticulate UO_2 and adsorbed U(VI) (Fig. 2, SI Table 1). Bulk UO_2 did not yield a good fit (SI Table 2) due to the strong U-U pair correlation present in the EXAFS spectra between ~ 8-12 $Å^{-1}$ for bulk UO_2 that is weaker in nanoparticulate UO_2.[32] In the presence of Ca, the GI-EXAFS spectra at both pH 5 and 10 were

best fit by sorbed U(VI) only. Under all sets of conditions, the GI-EXAFS could be confidently fit either by sorbed U(VI) alone (Ca present) or by a combination of sorbed U(VI) and nanoparticulate UO_2 (Ca absent); addition of other U(VI) phases did not improve the fit results, and in all cases resulted in a worse fit (i.e., fit features did not match spectral features, and the reduced χ^2 value increased). Examination of the spectral residuals (Fig. 2) shows that the remaining data (less than 5% of the total signal) is random noise, indicating that a potentially significant U-bearing phase has not been missed during the fitting routine. Discussion and comparison of the GI-EXAFS spectra Fourier transforms (SI. Fig. 5) are presented in the SI document.

The ability to spectroscopically distinguish simultaneously occurring adsorbed and precipitated U-bearing phases by linear-combination fitting of U L_{III}-edge XANES and EXAFS spectra has been previously shown, for example in systems with adsorbed U(VI) and U(VI)-bearing phosphates and silicates [5, 44], as well as systems with both simultaneous U(IV) and U(VI) present.[45] The presence of both nanoparticulate UO_2 and adsorbed U(VI) in the current study is supported by the GI-XANES spectra; in the absence of Ca, at both pH 5 and 10, the edge position of the GI-XANES spectra indicates that U reduction occurred, and that ~ 46-60 % of the total U present occurs as U(IV) (Table 1, SI Fig. 6). The amount of U(IV) present based on the LC fitting of the GI-EXAFS results is 35-42%. The minor difference between GI-XANES and GI-EXAFS could be due to the following factors: (1) the error associated with both the GI-XANES edge position and LCF protocol (both ~ ± 10 %) and (2) differences in sensitivity toward U(IV)- and U(VI)-bearing phases by the different spectroscopic geometries used to collect the reference spectra and the fitting techniques. Ultimately, the SEM, GI-XAS, and XPS analyses (SI Fig. 7) indicate that in the absence of Ca, both adsorption of U(VI) and reduction to

U(IV) and precipitation of nanoparticulate UO_2 occur simultaneously in adjacent regions of the magnetite surface. In the presence of Ca, no reduction occurred within error, and hence only adsorption of U(VI) is observed. It is therefore possible to elucidate the U(VI) coordination environment as there is only one dominant contribution to the GI-EXAFS spectra when Ca and CO_3 are present and no reduction occurred.

Direct identification of the U(IV)-bearing precipitates Scanning XRD patterns were collected in the grazing incidence geometry to confirm the identity of the U-bearing precipitates on the surface (SI Fig. 8). Under conditions in which no U reduction and precipitation occurred (with Ca and CO_3 present), as determined by GI-XAS and SEM, the only peaks present in the diffraction pattern are the magnetite (220) and (311) reflections (SI Fig. 8 A and C). These diffraction peaks result from a small degree of penetration and subsequent diffraction of the incident x-ray beam into the surface of the magnetite crystal. The observed (220) and (311) reflections are the first and third most intense diffraction peaks for magnetite.[46] Where U reduction and precipitation occurred (without Ca), as determined by GI-XAS and SEM, two additional peaks are observed which correspond to uraninite (111) and (200) (SI Fig. 8 B and D), the two most intense uraninite diffraction peaks.[47] These results, in combination with the SEM and GI-XAS data, confirm that when U reduction and surface precipitation occur, crystalline nanoparticulate UO_2 is the dominant U(IV)-bearing reaction product and co-exists with adsorbed uranyl. Although we cannot exclude the possibility of a small fraction (less than 5% of the total reduced U) of a non-uraninite U(IV)-bearing phase[48, 49], there was no x-ray diffraction or spectroscopic evidence to support the presence of such phases.

U(VI) adsorption complex analysis The LCF results above indicated that in the presence of Ca, at both pH 5 and 10, there was a single dominant U-bearing phase, specifically adsorbed U(VI). In the absence of a second contribution to the U L_{III}-edge GI-EXAFS spectra, shell-by-shell (SBS) fitting analyses of the sorption sample spectra reveal the coordination environment of the surface complex. The GI-EXAFS spectra and Fourier transform of the pH 5 and 10 sorption samples (Fig. 3) show subtle differences, particularly in the k range 7 to 9 $Å^{-1}$. The GI-EXAFS spectra of the pH 5 and 10 sorption samples were all fit with an axial oxygen shell at 1.799-1.802 ± 0.0003 Å, and a single equatorial oxygen shell at 2.37-2.39 ± 0.1 Å (Table 2). Use of a split equatorial oxygen shell did not produce a significantly improved fit to either spectra, although this splitting has been observed for other U(VI) surface complexes on Fe-bearing surfaces.[18, 50-53] Similar to these previous studies, the GI-EXAFS spectra were fit with an Fe shell (~ 2 Fe atoms at 3.70 Å) and a C shell (~ 2-3 C atoms at 2.94 Å). These results are consistent with a U(VI)-CO_3 surface species adsorbed in an inner-sphere configuration. The U-O_{eq} and U-Fe interatomic distances were used to constrain the geometry of the sorption complex based on the reported surface structure of magnetite (111).[26] Petitto et al. (2010) showed that for surface preparation and experimental condition similar to those used here, magnetite (111) is dominated by two oxygen terminated domains: 75% oxygen octahedral iron (OOI) termination and 25% oxygen mixed-iron (OMI) termination.[26] The OMI termination contains both ^{IV}Fe (tetrahedrally coordinated Fe, or equivalently A-sublattice Fe) and ^{VI}Fe (octahedrally coordinated Fe, or B-sublattice Fe) sites, and therefore U-O-Fe coordination environments on the OMI and OOI terminations can be expected to be different. Based on the GI-EXAFS spectra fit results, the U(VI) coordination environment can be best described as dominantly bidentate, likely

through two bridging equatorial oxygen atoms each to a different surface Fe site (i.e., biatomic-bidentate), with a spatial distribution over the surface in the ratio of ~ 60% OOI and ~ 40% OMI. This result is consistent with the coordination geometry of previously observed U(VI)-CO_3 sorption complexes.[25, 50, 51] The U(VI) sorption loading in the presence of both CO_3 and Ca was approximately 16 μmoles m^{-2} (Table 1), which is consistent with the formation of 1.2 monolayers of adsorbed U(VI) species assuming that all adsorbed U(VI) forms a U(VI)-CO_3-Ca surface complex. These high sorption loadings are likely the result of underestimating the magnetite (111) crystal surface area. The crystal surface area values ranged from $7.37x10^{-4}$ to $8.23x10^{-4}$ m^2 (SI). However, we could not accurately account for the exposed surface area on the sides of the magnetite crystals due to their rough nature, and these surfaces likely add up to an additional ~ 10-20 % reactive surface area. It is also possible that since there was no evidence for the precipitation of U(VI)-bearing solid phase, a small fraction of the total adsorbed U(VI) could be present as polynuclear surface species, although there was no evidence to support their presence in the GI-EXAFS spectra.

The fitting results also allow for U(VI) to be present by as much as 20% as a monodentate complex. Monodentate complexes are less likely, given the steric constraints of the non-complexed O_{eq} atoms bent upwards above the magnetite surface and the lower bond valence value of a surface oxygen atom bound to U(VI) in a monodentate coordination (1.79 v.u.) compared to the bidentate coordination (1.96 v.u.). Given the U-O and U-Fe interatomic distances, monodentate U(VI) would dominantly occur on the OMI layer, in contrast to the bidentate complex. The subtle differences in the GI-EXAFS spectra of the two sorption samples in the k range 7 to 9 $Å^{-1}$, can be attributed to differences in the U-Fe pair correlation. The GI-EXAFS spectrum of the pH 10 sample was fit with a slightly shorter U-Fe distance and slightly

greater coordination number compared to the pH 5 sample. These differences in the sorption complex coordination geometry at pH 5 and 10 could be due to more U(VI) sorbed on the OMI surface (and resulting sorption distribution ratio of ~ 45% OOI and ~ 55% OMI) and/or a slightly higher proportion of monodentate U(VI) (up to 25%).

The U-O, U-Fe, and U-C pair correlations were not sufficient to fully fit the GI-EXAFS spectra for the pH 5 and 10 sorption samples. Specifically, a peak feature in the Fourier transform at ~ 4 Å was confirmed to be a true single-scattering contribution and not multiple scattering or noise by continuous Cauchy wavelet transforms.[54] This contribution was fit with ~2 Ca atoms at 4.04 Å ± 0.3 Å. Although this region of the Fourier transform of U(VI) EXAFS spectra can be the result of single- and multiple-scattering contributions from distal oxygen atoms in the bound CO_3 groups[55], addition of these contributions to the model prior to or after adding the U-Ca pair correlation did not statistically improve the fit of this feature. An *F*-test was performed to determine the confidence level (*p*) of the SBS fit after including each additional shell. The p values after including each shell beyond the uranyl oxygen atoms were; 0.6 (C), 0.85 (Fe), and 0.95 (Ca), providing additional support for inclusion of the Ca shell. Although it remains unclear how Ca is bonded to the U(VI)-CO_3 surface complex, the proposed CO_3-Ca arrangement that results from constraining the U-O_{eq}, U-C, and U-Ca interatomic distances is consistent with the coordination environment for other Ca-CO_3-bearing phases with respect to interatomic distance and bond angles (Fig. 4). Further, the coordination environment of this proposed U(VI)-CO_3-Ca surface complex is consistent with the bulk EXAFS-determined atomic arrangement of aqueous U(VI)-CO_3-Ca complexes and that in the mineral liebigite ($Ca_2(UO_2)(CO_3)_3$•$11(H_2O)$).[55-57]

The ability to directly observe the presence of U(VI)-CO_3-Ca surface complexes has likely been hindered in previous work (e.g. reference [18]) due to the difficulty in detecting the U-Ca pair correlation, although such complexes has been invoked when modeling U(VI) sorption (e.g. [18, 58, 59]). The lower Fe fluorescence background and inherit surface sensitivity in GI-EXAFS compared to bulk EXAFS experiments, resulted in higher quality data leading to the possibility of detecting the presence of U-Ca pair correlation. For example, previous bulk EXAFS measurements with the U-PO_4-Ca system detected U-Ca nearest-neighbors, when there was no Fe fluorescence background.[44]

Simultaneous U adsorption and reduction Exposure of magnetite (111) to U(VI) in the presence of CO_3 and absence of Ca under batch conditions results in simultaneous adsorption of U(VI) and reduction of U(VI) to U(IV) and formation of nanoparticulate UO_2. The SEM analyses indicated that U reduction/precipitation occurred only at linear topographically negative features interpreted to be strained domain boundaries. In contrast, U(VI) adsorption presumably occurred along both the flat magnetite (111) surfaces and on domain boundaries and cracks walls. Restriction of reduction to domain boundaries and crack walls potentially explains some of the variability in results for U(VI) reduction by magnetite described in previous work. Specifically, the density of domain boundaries and other defects in the surface likely depend on the preparation method for both synthetic and natural samples, as well as variable inherent properties of natural crystals. Although not examined exhaustively, results from the current work indicate that single crystals with a high surface feature density (~ 20%) tended to yield higher U(IV)/U(VI) values after reaction compared to crystals with lower surface feature densities (~

10% or less). These results, in addition to previous work, indicate the U(VI) reduction by magnetite is controlled by the surface structure and stoichiometry[17], and defect concentration as well as the solution composition. This concept is further reinforced by recent computational molecular modeling studies. These studies indicate that the extent of U reduction on magnetite surfaces depends on the magnetite surface structure and Fe(II)/Fe(III) ratio[60], the local Fe(II) site density, the relative rates of electron conduction from the bulk to surface sites, and U coordination.[43]

Role of Ca and implications for U reactive transport modeling Results reported here indicate that prediction of retention by magnetite or release of U at a contaminated site requires understanding of the structure and stoichiometry of U surface species under a given set of conditions. The importance of aqueous U(VI)-CO_3-Ca ternary complexes under alkaline pH conditions has been observed in a variety of laboratory and field settings, as these complexes influence the fate of U(VI) in the environment by affecting both U(VI) adsorption and reduction.[20-22, 61] Differences in adsorption behavior is due in part to differences in the way U(VI) aqueous complexes can interact with a surface; a dominant U(VI)-CO_3-Ca aqueous complex, $Ca_2UO_2(CO_3)_3^0$, is neutrally charged, in contrast to mostly negatively charged U(VI)-hydrolysis and U(VI)-CO_3 complexes. Although the reduction mechanism and the effect of Ca during reduction remain unclear, it is obvious that Ca plays a major role in the fate of U in the environment. For example, bioremediation projects that aim to immobilize U via reduction and precipitation as insoluble UO_2 must first treat the groundwater to remove Ca.[62] Further, U(VI) can also form CO_3-ternary complexes with Mg such as $MgUO_2(CO_3)_3^{2-}$].[57] It is possible that

other alkaline earth uranyl carbonate, in addition to U(VI)-CO_3-Ca aqueous complexes, exhibit similar behavior with respect to U(VI) reduction.

It has previously been assumed that Ca has a less important role in affecting U mobility under acidic to circum-neutral pH conditions, where U(VI)-CO_3 and U(VI)-CO_3-Ca aqueous complexes are not predicted to dominate U speciation[63], and therefore U(VI) reduction under acidic conditions is not hampered by the presence of Ca and CO_3. However, the results presented here indicate that in fact, U(VI)-CO_3-Ca surface complexes can form at pH 5 under the conditions of our experiments. Although these complexes may not significantly affect the overall sorption/desorption behavior of U(VI), they inhibited U reduction on the magnetite (111) surface. If such inhibition occurs more broadly, some fundamental components in modeling U retention and release in the environment may need to be reconsidered. If U adsorption precedes Ca-complex formation, inhibition of U reduction indicates that complex formation is faster than reduction. Density functional theory calculations suggest that with Fe(II) bound to U(VI) through bridging axial oxygen atoms, the first electron transfer step is on the order of once per second[64], consistent with slow U(VI) reduction by Fe(II) in the presence of carbonate, in principle allowing time needed to form ternary U(VI)-CO_3-Ca complexes at the magnetite surface prior to and subsequently inhibiting U reduction. Further, the inhibition of U(VI) reduction in the presence of CO_3 and Ca at the surface might reflect slow kinetics of electron transfer (e.g., [64]), not necessarily thermodynamics, and that longer time frames need to be explored. Although further work is required to test these hypotheses, the present study indicates that this process can occur under a wider range of solution conditions than previously assumed. In summary, the results presented here represent the first direct spectroscopic evidence for U(VI)-CO_3-Ca surface complexes and provides insight into their structural topology. Further,

the reduction behavior of U(VI) at pH 5 depends strongly on the presence or absence of Ca and CO_3. The lack of significant aqueous U(VI)-CO_3-Ca complexes present in solution at acidic pH points strongly to a role for Ca at the magnetite-solution interface and that aqueous U(VI) does not need to be initially complexed with CO_3 and Ca in solution for heterogeneous surface reduction to be inhibited.

ACKNOWLEDGMENTS

We gratefully acknowledge support from the U.S. Department of Energy (DOE), Office of Science, Basic Energy Sciences (BES), under Contract No. DE-AC02-05CH11231. Portions of this work were carried out at the Advanced Photon Source (APS), the Environmental Molecular Sciences Laboratory (EMSL), and the Molecular Foundry (MF). Use of the APS was supported by the DOE-BES contract. DE-AC02-06CH11357. The EMSL is a national scientific user facility sponsored by the DOE Office of Biological and Environmental Research (BER). KMR and SMC acknowledge support from the DOE-BER Science Focus Area program at Pacific Northwest National Laboratory. ESI acknowledges support from the U.S. Department of Energy's Office of Basic Energy Sciences, Geosciences Program. Work at the MF was supported by the DOE-BES under contract DE-AC02-05CH11231. The authors would like to thank Peter Eng (APS) and Bruce Arey (EMSL) for their facilities support and assistance in data collection, and Joern Larsen (LBNL) for ICP analyses. Comments from four anonymous reviewers improved this manuscript.

Supporting Information Available

Additional information on the CMP protocol and post-CMP analysis for Fe_3O_4 (111), a picture of the GI-EXAFS samples cell, the multi-component LCF results, AFM images of the post-CMP magnetite crystals, batch experiment design, and XPS experimental setup and results is included in a Supporting Information document. This material is available free of charge via the Internet at http://pubs.acs.org.

TABLES

Table 1. Experimental, conditions, GI-XANES results, and U surface coverage.

GI-EXAFS sample conditions				
pH [a]	$[CO_3]_T$	[Ca]	U(IV) / U_T [b]	Γ (μmoles / m^2) [c]
5	0	0	0.60	22.34 ± 0.09
5	0.5 mM	0	0.49	21.27 ± 2.62
5	0.5 mM	0.1 mM	0.03	15.90 ± 0.68
10	0	0	0.47	25.23 ± 0.65
10	0.5 mM	0	0.46	28.67 ± 0.10
10	0.5 mM	0.1 mM	0.02	16.86 ± 1.12

a. All solutions contained 0.1 mM $UO_2(NO_3)_2$ and 1.0 mM $NaNO_3$; all Fe_3O_4 (111) samples exposed to solutions for 12 hours.

b. U(IV)/U_T determined from the energy position at ½E^0, with an error of ± 0.1.

c. Sorption loading, Γ, obtained from ICP measures of batch sorption experiments under similar conditions; error derived from 2SD of triplicate measurements. The crystal surface area values ranged from $7.37x10^{-4}$ to $8.23x10^{-4}$ m^2 (SI).

Table 2. Shell-by-shell fit results of the U L_{III}-edge GI-EXAFS spectra of magnetite(111) exposed to U(VI) at pH 5 and pH 10 in the presence of CO_3 and Ca.

	pH 5			pH 10		
Z	N [a]	R (Å) [b]	σ^2 (Å^2) [c]	N	R (Å)	σ^2 (Å^2)
O_{ax}	2.1(2)	1.802(6)	0.0016(3)	2.1(1)	1.799(1)	0.0003(1)
O_{eq}	6.4(5)	2.39(1)	0.007(2)	5.8(2)	2.37(2)	0.010(2)
C	3(1)	2.94(2)	0.003(2)	2(1)	2.95(3)	0.006(2)
Fe	2.0(5)	3.72(4)	0.007(3)	2.5(1)	3.68(2)	0.009(2)
Ca	2(1)	4.05(3)	0.008(4)	2.2(2)	4.03(4)	0.008(2)
ΔE^{0} [d]	8.0(5)			5.0(5)		
χ_v^2 [e]	16.4			11.2		

Note: The estimated standard deviations are listed in parentheses, representing the errors in the last digit; values without reported errors were fixed during fitting.

a. Coordination number

b. Interatomic distance

c. Debye-Waller factor

d. Difference in threshold Fermi level between data and theory

e. Reduced χ^2, a goodness-of-fit parameter[34]

FIGURE CAPTIONS

Figure 1. Representative SEM images of magnetite (111) exposed to a background electrolyte solution (1 mM $NaNO_3$) at pH 5 (A) and pH 10 (B), and to 0.1 mM U(VI) with no CO_3 and no Ca present at pH 5 (D-E) and pH 10 (G-H). The black dots on the SEM images are the location of where the EDS spectra were collected (see SI Fig. 4C, F, and I). Additional SEM images of magnetite exposed to U(VI) with CO_3 and no Ca present, and with CO_3 and with Ca present can be found in SI Fig. 5.

Figure 2. Best fit results (dashed gray lines) by least-squares linear combination fitting of the U L_{III}-edge GI-EXAFS spectra (solid lines) and residuals (light gray line). The best-fit components are uranyl sorbed to chlorite and nanoparticulate UO_2; tabulated best-fit results are presented in SI Table 1 and additional multi-component fit results are tabulated in SI Table 2.

Figure 3. U L_{III}-edge GI-EXAFS spectra (solid line) and fits (dashed lines) of magnetite(111) exposed to U(VI) at pH 5 and pH 10 in the presence of CO_3 and Ca at left, and Fourier transform at right. In the Fourier transform plots, the vertical lines represent the position of the first shell of axial oxygen atoms (O_{ax}), second shell of equatorial oxygen atoms (O_{eq}), third shell of carbon atoms, fourth shell of Fe atoms, and fifth shell of Ca atoms.

Figure 4. Schematic drawing of the likely dominant bidentate U(VI)-CO_3-Ca sorption complex on the OOI surface of magnetite (111); U(VI) (cross-hatched), oxygen (equatorial lined), carbon (white), tetrahedral iron (black), octahedral iron (gray), and calcium (striped). The full complex is not shown on the OMI surface, in order to illustrate the potential positions of U(VI).

FIGURES

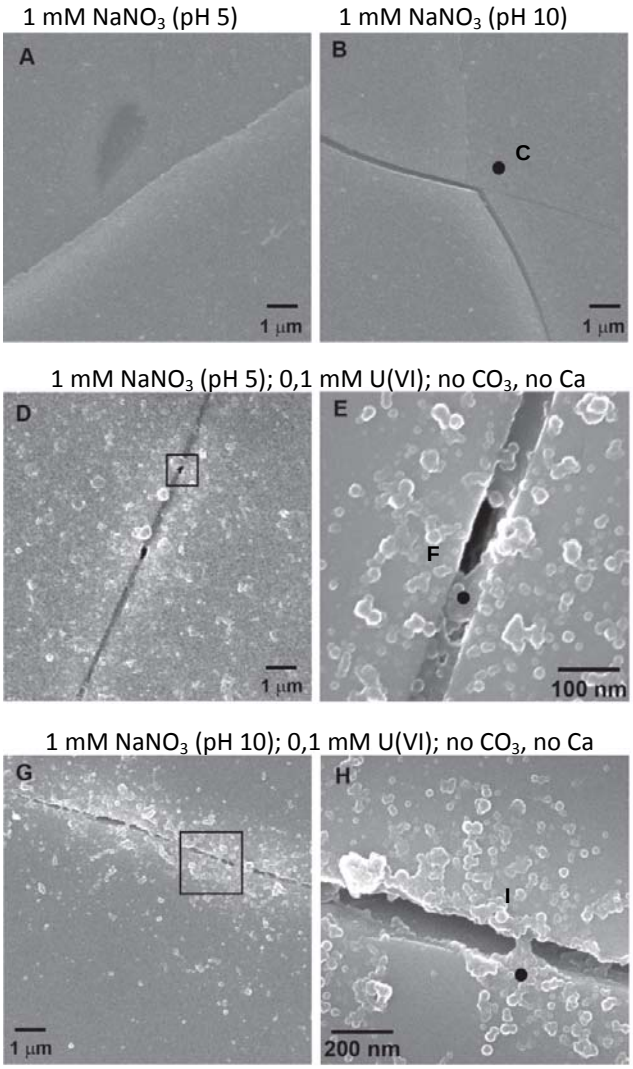

Figure 1. Representative SEM images of magnetite (111) exposed to a background electrolyte solution (1 mM $NaNO_3$) at pH 5 (A) and pH 10 (B), and to 0.1 mM U(VI) with no CO_3 and no Ca present at pH 5 (D-E) and pH 10 (G-H). The black dots on the SEM images are the location of where the EDS spectra were collected (see SI Fig. 4C, F, and I). Additional SEM images of magnetite exposed to U(VI) with CO_3 and no Ca present, and with CO_3 and Ca present can be found in SI Fig. 5.

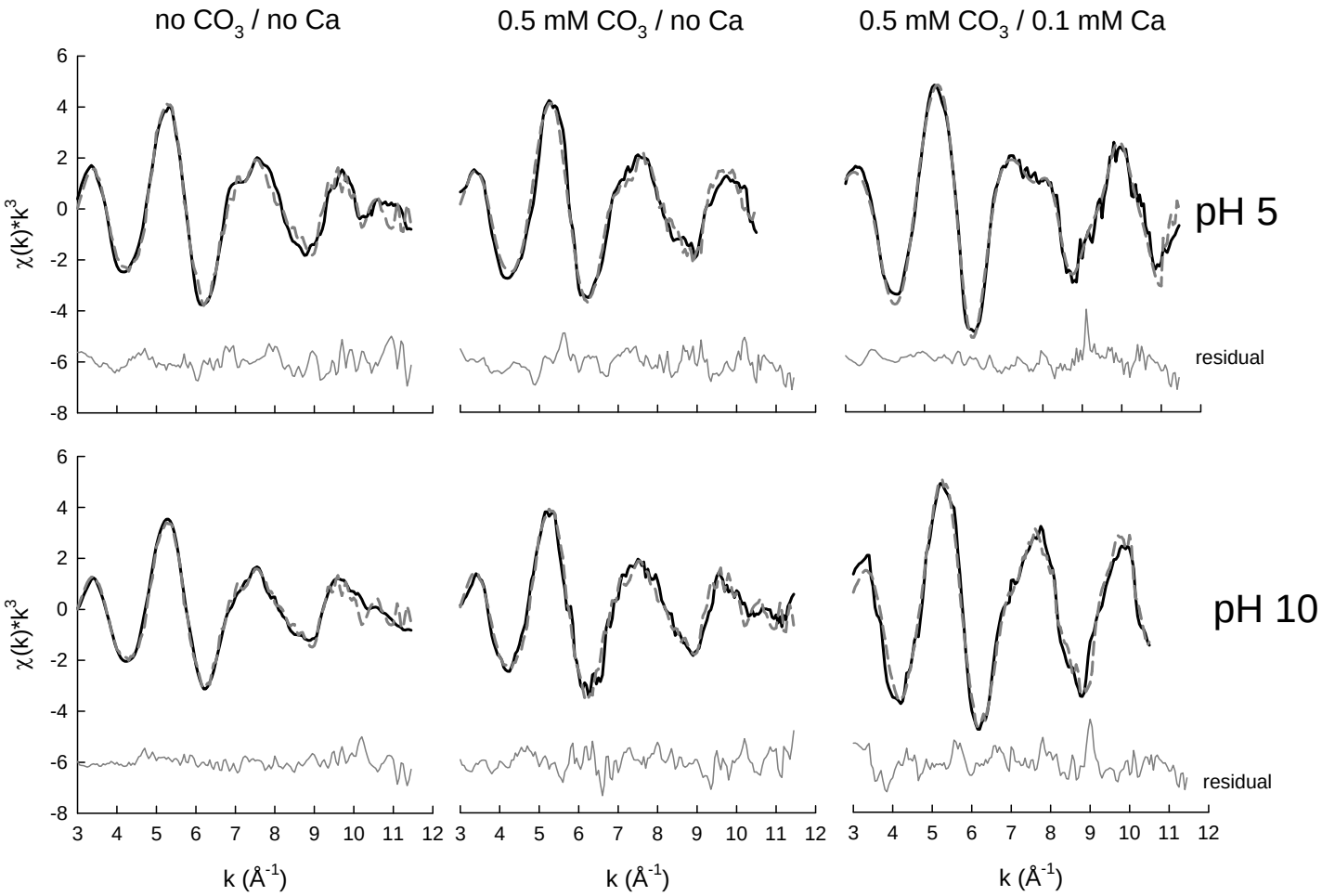

Figure 2. Best fit results (dashed gray lines) by least-squares linear combination fitting of the U L_{III}-edge GI-EXAFS spectra (solid lines) and residuals (light gray line). The best-fit components are uranyl sorbed to chlorite and nanoparticulate UO_2; tabulated best-fit results are presented in SI Table 2 and additional multi-component fit results are tabulated in SI Table 2.

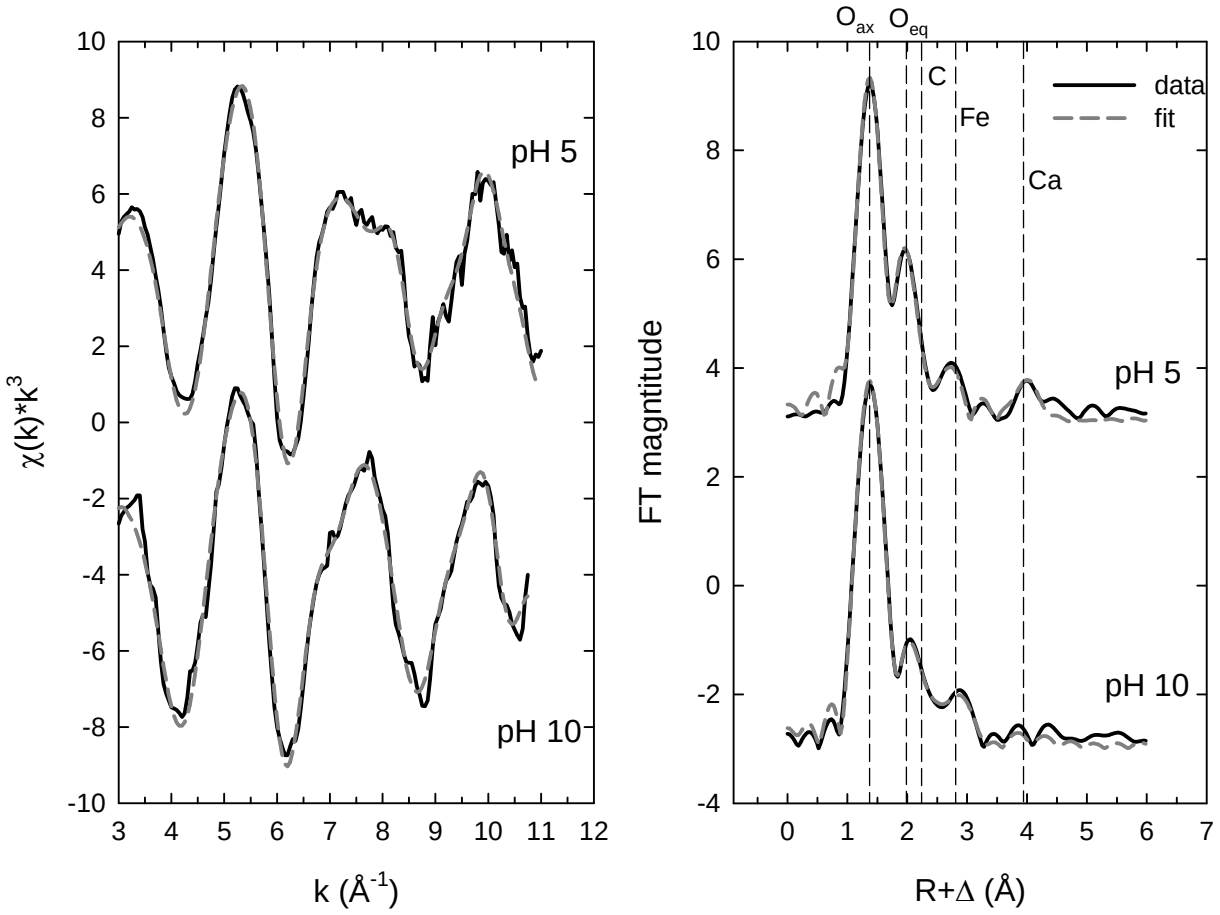

Figure 3. U L_{III}-edge GI-EXAFS spectra (solid line) and fits (dashed lines) of magnetite(111) exposed to U(VI) at pH 5 and pH 10 in the presence of CO_3 and Ca at left, and Fourier transform at right. In the Fourier transform plots, the vertical lines represent the position of the first shell of axial oxygen atoms (O_{ax}), second shell of equatorial oxygen atoms (O_{eq}), third shell of carbon atoms, fourth shell of Fe atoms, and fifth shell of Ca atoms.

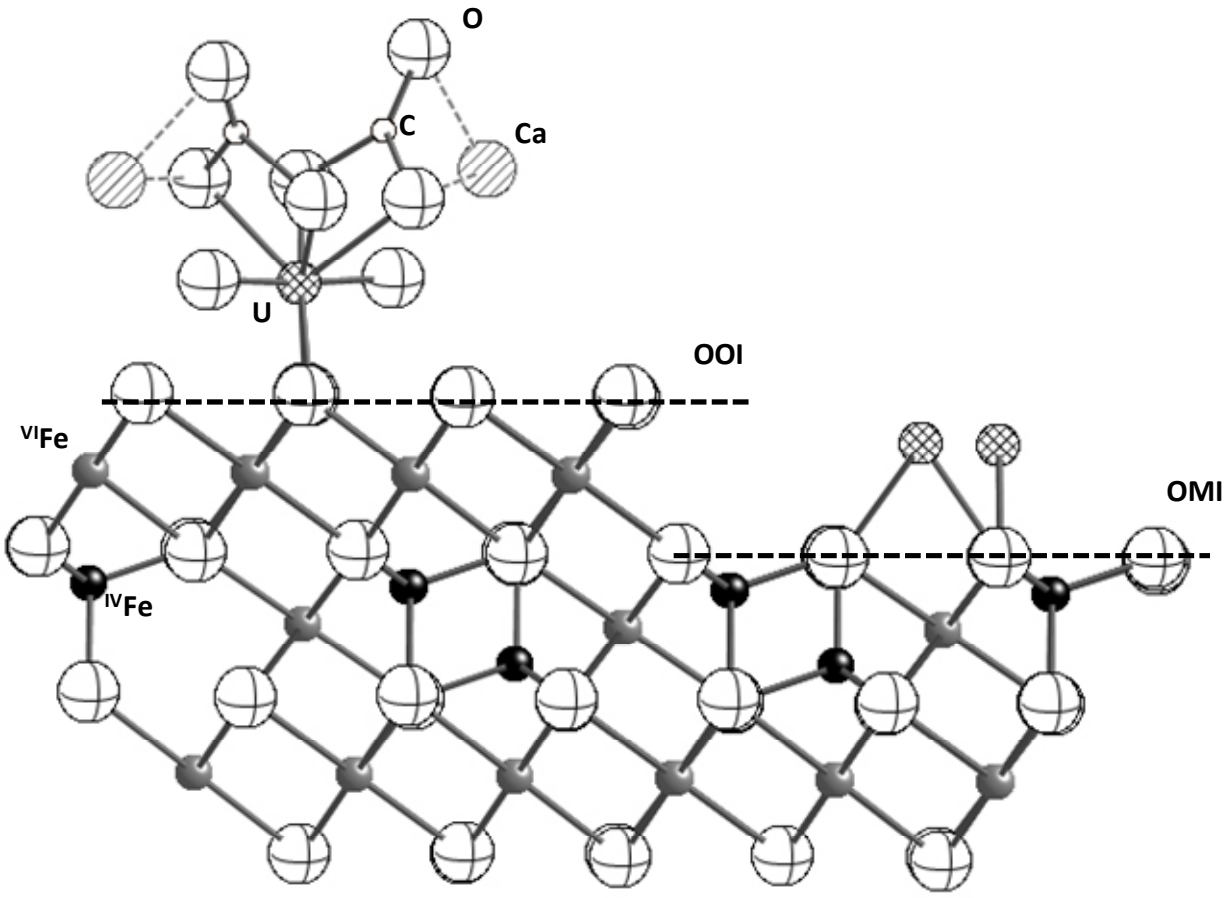

Figure 4. Schematic drawing of the likely dominant bidentate U(VI)-CO_3-Ca sorption complex on the OOI surface of magnetite (111); U(VI) (cross-hatched), oxygen (equatorial lined), carbon (white), tetrahedral iron (black), octahedral iron (gray), and calcium (striped). The full complex is not shown on the OMI surface, in order to illustrate the potential positions of U(VI).

REFERENCES

1. Riley, R. G.; Zachara, J. M.; Wobber, F. J. *Chemical contaminants on DOE lands and selection of contaminant mixtures for subsurface science research DOE/ER-0547T*; DOE/ER-0547T; U.S. Department of Energy: Washington, D.C., April 1992, 1992.

2. Veeramani, H.; Alessi, D. S.; Suvorova, E. I.; Lezama-Pacheco, J. S.; Stubbs, J. E.; Sharp, J. O.; Dippon, U.; Kappler, A.; Bargar, J. R.; Bernier-Latmani, R., Products of abiotic U(VI) reduction by biogenic magnetite and vivianite. *Geochim. Cosmochim. Acta* **2011,** *75*, (9), 2512-2528.

3. Vikesland, P. J.; Valentine, R. L., Iron oxide surface-catalyzed oxidation of ferrous iron by monochloramine: Implications of oxide type and carbonate on reactivity. *Environ. Sci. Technol.* **2002,** *36*, (3), 512-519.

4. Watts, R. J.; Udell, M. D.; Kong, S.; Leung, S. W., Fenton-like soil remediation catalyzed by naturally occurring iron minerals. *Environ. Eng. Sci.* **1999,** *16*, (1), 93-103.

5. Singer, D. M.; Zachara, J. M.; Brown Jr, G. E., Uranium speciation as a function of depth in contaminated Hanford sediments - A micro-XRF, micro-XRD, and micro- and bulk-XAFS Study. *Environ. Sci. Technol.* **2009,** *43*, (3), 630-636.

6. Duro, L.; El Aamrani, S.; Rovira, M.; de Pablo, J.; Bruno, J., Study of the interaction between U(VI) and the anoxic corrosion products of carbon steel. *Appl. Geochem.* **2008,** *23*, (5), 1094-1100.

7. Shipley, H. J.; Yean, S.; Kan, A. T.; Tomson, M. B., Adsorption of arsenic to magnetite nanoparticles: Effect of particle concentration, pH, ionic strength, and temperature. *Environ. Toxicol. Chem.* **2009,** *28*, (3), 509-515.

8. Doyle, C. S.; Kendelewicz, T.; Brown Jr, G. E., Inhibition of the reduction of Cr(VI) at the magnetite-water interface by calcium carbonate coatings. *Appl. Surf. Sci.* **2004,** *230*, (1-4), 260-271.

9. Jung, Y.; Choi, J.; Lee, W., Spectroscopic investigation of magnetite surface for the reduction of hexavalent chromium. *Chemosphere* **2007,** *68*, (10), 1968-1975.

10. Wiatrowski, H. A.; Das, S.; Kukkadapu, R.; Ilton, E. S.; Barkay, T.; Yee, N., Reduction of Hg(II) to Hg(0) by magnetite. *Environ. Sci. Technol.* **2009,** *43*, (14), 5307-5313.

11. Regenspurg, S.; Schild, D.; Schäfer, T.; Huber, F.; Malmström, M. E., Removal of uranium(VI) from the aqueous phase by iron(II) minerals in presence of bicarbonate. *Appl. Geochem.* **2009,** *24*, (9), 1617-1625.

12. Jeon, B.-H.; Dempsey, B. A.; Burgos, W. D.; Barnett, M. O.; Roden, E. E., Chemical reduction of U(VI) by Fe(II) at the solid-water interface using natural and synthetic Fe(III) oxides. *Environ. Sci. Technol.* **2005,** *39*, (15), 5642-5649.

13. Scott, T. B.; Allen, G. C.; Heard, P. J.; Randell, M. G., Reduction of U(VI) to U(IV) on the surface of magnetite. *Geochim. Cosmochim. Acta* **2005,** *69*, (24), 5639-5646.

14. Missana, T.; García-Gutiérrez, M.; Fernndez, V., Uranium (VI) sorption on colloidal magnetite under anoxic environment: Experimental study and surface complexation modelling. *Geochim. Cosmochim. Acta* **2003,** *67*, (14), 2543-2550.

15. Missana, T.; Maffiotte, C.; García-Gutiérrez, M., Surface reactions kinetics between

nanocrystalline magnetite and uranyl. *J. Colloid Interface Sci.* **2003,** *261*, 154-160.

16. Ilton, E. S.; Boily, J.-F.; Buck, E. C.; Skomurski, F. N.; Rosso, K. M.; Cahill, C. L.; Bargar, J. R.; Felmy, A. R., Influence of dynamical conditions on the reduction of U^{VI} at the magnetite-solution interface. *Environ. Sci. Technol.* **2010,** *44*, (1), 170-176.

17. Singer, D. M.; Maher, K.; Brown Jr, G. E., Uranyl-chlorite sorption/desorption: Evaluation of different U(VI) sequestration processes. *Geochim. Cosmochim. Acta* **2009,** *73*, (20), 5989-6007.

18. Lovley, D. R.; Phillips, E. J. P.; Gorby, Y. A.; Landa, E. R., Microbial reduction of uranium. *Nature* **1991,** *350*, (6317), 413-416.

19. Brooks, S. C.; Fredrickson, J. K.; Carroll, S. L.; Kennedy, D. W.; Zachara, J. M.; Plymale, A. E.; Kelly, S. D.; Kemner, K. M.; Fendorf, S., Inhibition of bacterial U(VI) reduction by calcium. *Environ. Sci. Technol.* **2003,** *37*, (9), 1850-1858.

20. Liu, C.; Jeon, B.-H.; Zachara, J. M.; Wang, Z., Influence of calcium on microbial reduction of solid phase uranium(VI). *Biotechnol. Bioeng.* **2007,** *97*, (6), 1415-1422.

21. Stewart, B. D.; Neiss, J.; Fendorf, S., Quantifying constraints imposed by calcium and iron on bacterial reduction of uranium(VI). *J Environ. Qual.* **2007,** *36*, (2), 363-372.

22. Waychunas, G.; Trainor, T.; Eng, P.; Catalano, J.; Brown Jr, G. E.; Davis, J.; Rogers, J.; Bargar, J., Surface complexation studied via combined grazing-incidence EXAFS and surface diffraction: arsenate on hematite (0001) and (10-12). *Anal. Bioanal. Chem.* **2005,** *383*, (1), 12-27.

23. Greaves, G. N.; Barrett, N. T.; Antonini, G. M.; Thornley, F. R.; Willis, B. T. M.; Steel, A., Glancing-angle X-ray absorption spectroscopy of corroded borosilicate glass surfaces containing uranium. *JACS* **1989,** *111*, (12), 4313-4324.

24. Catalano, J. G.; Trainor, T. P.; Eng, P. J.; Waychunas, G. A.; Brown Jr, G. E., CTR diffraction and grazing-incidence EXAFS study of U(VI) adsorption onto α-Al_2O_3 and α-Fe_2O_3 (11-02) surfaces. *Geochim. Cosmochim. Acta* **2005,** *69*, (14), 3555-3572.

25. Clark, T. M.; Evans, B. J., Influence of chemical composition on the crystalline morphologies of magnetite. *IEEE Trans. Magn.* **1997,** *33*, (5), 4257-4259.

26. Petitto, S. C.; Tanwar, K. S.; Ghose, S. K.; Eng, P. J.; Trainor, T. P., Surface structure of magnetite (111) under hydrated conditions by crystal truncation rod diffraction. *Surf. Sci.* **2010,** *604*, (13-14), 1082-1093.

27. Özdemir, Ö.; Dunlop, D. J., Magnetic domain structures on a natural single crystal of magnetite. *Geophys. Res. Lett.* **1993,** *20*, (17), 1835-1838.

28. Özdemir, Ö.; Xu, S.; Dunlop, D. J., Closure domains in magnetite. *J. Geophys. Res.* **1995,** *100*, (B2), 2193-2209.

29. Özdemir, Ö.; Dunlop, D. J., Effect of crystal defects and internal stress on the domain structure and magnetic properties of magnetite. *J. Geophys. Res.* **1997,** *102*, (B9), 20211-20224.

30. Newville, M.; Sutton, S. R.; Rivers, M. L.; Eng, P., Micro-beam x-ray absorption and fluorescence spectroscopies at GSECARS: APS beamline 13ID. *J. Synchrotron Rad.* **1999,** *6*, (3), 353-355.

31. Singer, D. M.; Farges, F.; Brown Jr, G. E., Biogenic nanoparticulate UO_2: Synthesis,

characterization, and factors affecting surface reactivity. *Geochim. Cosmochim. Acta* **2009,** *73*, (12), 3593-3611.

32. Webb, S., SixPACK: a graphical user interface for XAS analysis using IFEFFIT. *Phys. Scr.* **2004,** *T115*, 1011-1014.

33. Newville, M., IFEFFIT: interactive XAFS analysis and FEFF fitting. *Journal of Synchrotron Radiation* **2001,** *8*, 322-324.

34. Manceau, A.; Marcus, M. A.; Tamura, N., Quantitative speciation of heavy metals in soils and sediments by synchrotron X-ray techniques. In *Reviews in Mineralogy and Geochemistry V.49*, Rosso, J. J.; Ribbe, P. H., Eds. Geochemical Society of America: Washington, D.C., 2002; Vol. 49.

35. Catalano, J. G.; McKinley, J. P.; Zachara, J. M.; Heald, S. M.; Smith, S. C.; Brown Jr, G. E., Changes in uranium speciation through a depth sequence of contaminated Hanford sediments. *Environ. Sci. Technol.* **2006,** *40*, (8), 2517 -2524.

36. Catalano, J. G.; Brown Jr, G. E., Analysis of uranyl-bearing phases by EXAFS spectroscopy: Interferences, multiple scattering, accuracy of structural parameters, and spectral differences. *Am. Mineral.* **2004,** *89*, 1004-1021.

37. Ankudinov, A. L.; Rehr, J. J., Relativistic calculations of spin-dependent x-ray-absorption spectra. *Physical Review B* **1997,** *56*, (4), R1712 LP - R1716.

38. Demartin, F.; Gramaccioli, C. M.; Pilati, T., The importance of accurate crystal structure determination of uranium minerals. II. Soddyite $(UO_2)_2(SiO_4)\cdot 2H_2O$. *Acta Crystallographica Section C* **1992,** *48*, (1), 1-4.

39. Mereiter, K., The crystal structure of Liebigite, $Ca_2UO_2(CO_3)_3\cdot\sim 11H_2O$. *Tschermaks Min. Petr. Mitt.* **1982,** *30*, (4), 277-288.

40. Piret, P.; Piret-Meunier, J.; Declercq, J.-P., Structure of phuralumite. *Acta Crystallographica Section B* **1979,** *35*, (8), 1880-1882.

41. Skomurski, F. N.; Ilton, E. S.; Engelhard, M. H.; Arey, B. W.; Rosso, K. M., Heterogeneous reduction of U^{6+} by structural Fe^{2+} from theory and experiment. *Geochim. Cosmochim. Acta In Press*.

42. Fuller, C. C.; Bargar, J. R.; Davis, J. A.; Piana, M. J., Mechanisms of uranium interactions with hydroxyapatite: Implications for groundwater remediation. *Environ. Sci. Technol.* **2002,** *36*, (2), 158-165.

43. Chakraborty, S.; Favre, F.; Banerjee, D.; Scheinost, A. C.; Mullet, M.; Ehrhardt, J.-J.; Brendle, J.; Vidal, L. c.; Charlet, L., U(VI) sorption and reduction by Fe(II) sorbed on montmorillonite. *Environ. Sci. Technol.* **2010,** *44*, (10), 3779-3785.

44. Fleet, M., The structure of magnetite. *Acta Crystallographica Section B* **1981,** *37*, (4), 917-920.

45. Wyckoff, R. W. G., *Crystal Structures 1 Second edition*. Interscience Publishers: New York, New York, 1963; p 239-444.

46. Bargar, J. R.; Reitmeyer, R.; Davis, J. A., Spectroscopic confirmation of uranium(VI)-carbonato adsorption complexes on hematite. *Environ. Sci. Technol.* **1999,** *33*, (14), 2481-2484.

47. Bargar, J. R.; Reitmeyer, R.; Lenhart, J. J.; Davis, J. A., Characterization of U(VI)-carbonato ternary complexes on hematite: EXAFS and electrophoretic mobility measurements. *Geochim.*

Cosmochim. Acta **2000,** *64*, (16), 2737-2749.

48. Catalano, J. G.; Brown Jr., G. E., Uranyl adsorption onto montmorillonite: Evaluation of binding sites and carbonate complexation. *Geochim. Cosmochim. Acta* **2005,** *69*, (12), 2995-3005.

49. Sylwester, E. R.; Hudson, E. A.; Allen, P. G., The structure of uranium(VI) sorption complexes on silica, alumina, and montmorillonite. *Geochim. Cosmochim. Acta* **2000,** *64*, (14), 2431-2438.

50. Muñoz, M.; Argoul, P.; Farges, F., Continuous Cauchy wavelet transform analyses of EXAFS spectra: A qualitative approach. *Am. Mineral.* **2003,** *88*, 694-700.

51. Bernhard, G.; Geipel, G.; Reich, T.; Brendler, V.; Amayri, S.; Nitsche, H., Uranyl(VI) carbonate complex formation: Validation of the $Ca_2UO_2(CO_3)_3$(aq.) species. *Radiochim. Acta* **2001,** *89*, (8), 511-518.

52. Amayri, S.; Reich, T.; Arnold, T.; Geipel, G.; Bernhard, G., Spectroscopic characterization of alkaline earth uranyl carbonates. *J. Solid State Chem.* **2005,** *178*, (2), 567-577.

53. Kelly, S. D.; Kemner, K. M.; Brooks, S. C., X-ray absorption spectroscopy identifies calcium-uranyl-carbonate complexes at environmental concentrations. *Geochim. Cosmochim. Acta* **2007,** *71*, (4), 821-834.

54. Gorman-Lewis, D.; Elias, P. E.; Fein, J. B., Adsorption of aqueous uranyl complexes onto *Bacillus subtilis* cells. *Environ. Sci. Technol.* **2005,** *39*, (13), 4906-4912.

55. Sheng, L.; Szymanowski, J.; Fein, J. B., The effects of uranium speciation on the rate of U(VI) reduction by *Shewanella oneidensis* MR-1. *Geochim. Cosmochim. Acta* **2011,** *75*, (12), 3558-3567.

56. Skomurski, F. N.; Kerisit, S.; Rosso, K. M., Structure, charge distribution, and electron hopping dynamics in magnetite (Fe_3O_4) (1 0 0) surfaces from first principles. *Geochim. Cosmochim. Acta* **2010,** *74*, (15), 4234-4248.

57. Fox, P. M.; Davis, J. A.; Zachara, J. M., The effect of calcium on aqueous uranium(VI) speciation and adsorption to ferrihydrite and quartz. *Geochim. Cosmochim. Acta* **2006,** *70*, (6), 1379-1387.

58. Wu, W. M.; Carley, J.; Fienen, M.; Mehlhorn, T.; Lowe, K.; Nyman, J.; Luo, J.; Gentile, M. E.; Rajan, R.; Wagner, D.; Hickey, R. F.; Gu, B. H.; Watson, D.; Cirpka, O. A.; Kitanidis, P. K.; Jardine, P. M.; Criddle, C. S., Pilot-scale in situ bioremediation of uranium in a highly contaminated aquifer. 1. Conditioning of a treatment zone. *Environ. Sci. Technol.* **2006,** *40*, (12), 3978-3985.

59. Guillaumont, R.; Fanghänel, T.; Fuger, J.; Grenthe, I.; Neck, V.; Palmer, D. A.; Rand, M. H., *Update on the Chemical Thermodynamics of Uranium, Neptunium, Plutonium, Americium and Technetium*. Elsevier: Amsterdam, 2003; Vol. 5.

60. Wander, M. C. F.; Kerisit, S.; Rosso, K. M.; Schoonen, M. A. A., Kinetics of triscarbonato uranyl reduction by aqueous ferrous iron: A theoretical study. *J. Phys. Chem. A* **2006,** *110*, (31), 9691-9701.

1. Riley, R. G.; Zachara, J. M.; Wobber, F. J. *Chemical contaminants on DOE lands and selection of contaminant mixtures for subsurface science research DOE/ER-0547T*; DOE/ER-0547T; U.S. Department of Energy: Washington, D.C., April 1992, 1992.
2. Veeramani, H.; Alessi, D. S.; Suvorova, E. I.; Lezama-Pacheco, J. S.; Stubbs, J. E.; Sharp, J. O.; Dippon, U.; Kappler, A.; Bargar, J. R.; Bernier-Latmani, R., Products of abiotic U(VI) reduction by biogenic magnetite and vivianite. *Geochim. Cosmochim. Acta* **2011,** *75*, (9), 2512-2528.
3. Vikesland, P. J.; Valentine, R. L., Iron oxide surface-catalyzed oxidation of ferrous iron by monochloramine: Implications of oxide type and carbonate on reactivity. *Environ. Sci. Technol.* **2002,** *36*, (3), 512-519.
4. Watts, R. J.; Udell, M. D.; Kong, S.; Leung, S. W., Fenton-like soil remediation catalyzed by naturally occurring iron minerals. *Environ. Eng. Sci.* **1999,** *16*, (1), 93-103.
5. Singer, D. M.; Zachara, J. M.; Brown Jr, G. E., Uranium speciation as a function of depth in contaminated Hanford sediments - A micro-XRF, micro-XRD, and micro- and bulk-XAFS Study. *Environ. Sci. Technol.* **2009,** *43*, (3), 630-636.
6. Duro, L.; El Aamrani, S.; Rovira, M.; de Pablo, J.; Bruno, J., Study of the interaction between U(VI) and the anoxic corrosion products of carbon steel. *Appl. Geochem.* **2008,** *23*, (5), 1094-1100.
7. Shipley, H. J.; Yean, S.; Kan, A. T.; Tomson, M. B., Adsorption of arsenic to magnetite nanoparticles: Effect of particle concentration, pH, ionic strength, and temperature. *Environ. Toxicol. Chem.* **2009,** *28*, (3), 509-515.
8. Doyle, C. S.; Kendelewicz, T.; Brown Jr, G. E., Inhibition of the reduction of Cr(VI) at the magnetite-water interface by calcium carbonate coatings. *Appl. Surf. Sci.* **2004,** *230*, (1-4), 260-271.
9. Jung, Y.; Choi, J.; Lee, W., Spectroscopic investigation of magnetite surface for the reduction of hexavalent chromium. *Chemosphere* **2007,** *68*, (10), 1968-1975.
10. Wiatrowski, H. A.; Das, S.; Kukkadapu, R.; Ilton, E. S.; Barkay, T.; Yee, N., Reduction of Hg(II) to Hg(0) by magnetite. *Environ. Sci. Technol.* **2009,** *43*, (14), 5307-5313.
11. Regenspurg, S.; Schild, D.; Schäfer, T.; Huber, F.; Malmström, M. E., Removal of uranium(VI) from the aqueous phase by iron(II) minerals in presence of bicarbonate. *Appl. Geochem.* **2009,** *24*, (9), 1617-1625.
12. Jeon, B.-H.; Dempsey, B. A.; Burgos, W. D.; Barnett, M. O.; Roden, E. E., Chemical reduction of U(VI) by Fe(II) at the solid-water interface using natural and synthetic Fe(III) oxides. *Environ. Sci. Technol.* **2005,** *39*, (15), 5642-5649.
13. Scott, T. B.; Allen, G. C.; Heard, P. J.; Randell, M. G., Reduction of U(VI) to U(IV) on the surface of magnetite. *Geochim. Cosmochim. Acta* **2005,** *69*, (24), 5639-5646.
14. Missana, T.; García-Gutiérrez, M.; Fernndez, V., Uranium (VI) sorption on colloidal magnetite under anoxic environment: Experimental study and surface complexation modelling. *Geochim. Cosmochim. Acta* **2003,** *67*, (14), 2543-2550.
15. Missana, T.; Maffiotte, C.; García-Gutiérrez, M., Surface reactions kinetics between nanocrystalline magnetite and uranyl. *J. Colloid Interface Sci.* **2003,** *261*, 154-160.
16. Ilton, E. S.; Boily, J.-F.; Buck, E. C.; Skomurski, F. N.; Rosso, K. M.; Cahill, C. L.; Bargar, J. R.; Felmy, A. R., Influence of dynamical conditions on the reduction of U^{VI} at the magnetite-solution interface. *Environ. Sci. Technol.* **2010,** *44*, (1), 170-176.
17. Gorski, C. A.; Nurmi, J. T.; Tratnyek, P. G.; Hofstetter, T. B.; Scherer, M. M., Redox behavior of magnetite: Implications for contaminant reduction. *Environ. Sci. Technol.* **2009,** *44*, (1), 55-60.
18. Singer, D. M.; Maher, K.; Brown Jr, G. E., Uranyl-chlorite sorption/desorption: Evaluation of different U(VI) sequestration processes. *Geochim. Cosmochim. Acta* **2009,** *73*, (20), 5989-6007.
19. Lovley, D. R.; Phillips, E. J. P.; Gorby, Y. A.; Landa, E. R., Microbial reduction of uranium. *Nature* **1991,** *350*, (6317), 413-416.
20. Brooks, S. C.; Fredrickson, J. K.; Carroll, S. L.; Kennedy, D. W.; Zachara, J. M.; Plymale, A. E.; Kelly, S. D.; Kemner, K. M.; Fendorf, S., Inhibition of bacterial U(VI) reduction by calcium. *Environ. Sci. Technol.* **2003,** *37*, (9), 1850-1858.
21. Liu, C.; Jeon, B.-H.; Zachara, J. M.; Wang, Z., Influence of calcium on microbial reduction of

solid phase uranium(VI). *Biotechnol. Bioeng.* **2007,** *97*, (6), 1415-1422.
22. Stewart, B. D.; Neiss, J.; Fendorf, S., Quantifying constraints imposed by calcium and iron on bacterial reduction of uranium(VI). *J Environ. Qual.* **2007,** *36*, (2), 363-372.
23. Waychunas, G.; Trainor, T.; Eng, P.; Catalano, J.; Brown Jr, G. E.; Davis, J.; Rogers, J.; Bargar, J., Surface complexation studied via combined grazing-incidence EXAFS and surface diffraction: arsenate on hematite (0001) and (10-12). *Anal. Bioanal. Chem.* **2005,** *383*, (1), 12-27.
24. Greaves, G. N.; Barrett, N. T.; Antonini, G. M.; Thornley, F. R.; Willis, B. T. M.; Steel, A., Glancing-angle X-ray absorption spectroscopy of corroded borosilicate glass surfaces containing uranium. *JACS* **1989,** *111*, (12), 4313-4324.
25. Catalano, J. G.; Trainor, T. P.; Eng, P. J.; Waychunas, G. A.; Brown Jr, G. E., CTR diffraction and grazing-incidence EXAFS study of U(VI) adsorption onto α-Al_2O_3 and α-Fe_2O_3 (11-02) surfaces. *Geochim. Cosmochim. Acta* **2005,** *69*, (14), 3555-3572.
26. Petitto, S. C.; Tanwar, K. S.; Ghose, S. K.; Eng, P. J.; Trainor, T. P., Surface structure of magnetite (111) under hydrated conditions by crystal truncation rod diffraction. *Surf. Sci.* **2010,** *604*, (13-14), 1082-1093.
27. Clark, T. M.; Evans, B. J., Influence of chemical composition on the crystalline morphologies of magnetite. *IEEE Trans. Magn.* **1997,** *33*, (5), 4257-4259.
28. Özdemir, Ö.; Dunlop, D. J., Magnetic domain structures on a natural single crystal of magnetite. *Geophys. Res. Lett.* **1993,** *20*, (17), 1835-1838.
29. Özdemir, Ö.; Xu, S.; Dunlop, D. J., Closure domains in magnetite. *J. Geophys. Res.* **1995,** *100*, (B2), 2193-2209.
30. Özdemir, Ö.; Dunlop, D. J., Effect of crystal defects and internal stress on the domain structure and magnetic properties of magnetite. *J. Geophys. Res.* **1997,** *102*, (B9), 20211-20224.
31. Newville, M.; Sutton, S. R.; Rivers, M. L.; Eng, P., Micro-beam x-ray absorption and fluorescence spectroscopies at GSECARS: APS beamline 13ID. *J. Synchrotron Rad.* **1999,** *6*, (3), 353-355.
32. Singer, D. M.; Farges, F.; Brown Jr, G. E., Biogenic nanoparticulate UO_2: Synthesis, characterization, and factors affecting surface reactivity. *Geochim. Cosmochim. Acta* **2009,** *73*, (12), 3593-3611.
33. Webb, S., SixPACK: a graphical user interface for XAS analysis using IFEFFIT. *Phys. Scr.* **2004,** *T115*, 1011-1014.
34. Newville, M., IFEFFIT: interactive XAFS analysis and FEFF fitting. *J. Synchrotron Rad.* **2001,** *8*, 322-324.
35. Manceau, A.; Marcus, M. A.; Tamura, N., Quantitative speciation of heavy metals in soils and sediments by synchrotron X-ray techniques. In *Reviews in Mineralogy and Geochemistry V.49*, Rosso, J. J.; Ribbe, P. H., Eds. Geochemical Society of America: Washington, D.C., 2002; Vol. 49.
36. Catalano, J. G.; McKinley, J. P.; Zachara, J. M.; Heald, S. M.; Smith, S. C.; Brown Jr, G. E., Changes in uranium speciation through a depth sequence of contaminated Hanford sediments. *Environ. Sci. Technol.* **2006,** *40*, (8), 2517 -2524.
37. Catalano, J. G.; Brown Jr, G. E., Analysis of uranyl-bearing phases by EXAFS spectroscopy: Interferences, multiple scattering, accuracy of structural parameters, and spectral differences. *Am. Mineral.* **2004,** *89*, 1004-1021.
38. Ankudinov, A. L.; Rehr, J. J., Relativistic calculations of spin-dependent x-ray-absorption spectra. *Physical Review B* **1997,** *56*, (4), R1712 LP - R1716.
39. Demartin, F.; Gramaccioli, C. M.; Pilati, T., The importance of accurate crystal structure determination of uranium minerals. II. Soddyite $(UO_2)_2(SiO_4)\cdot 2H_2O$. *Acta Crystallographica Section C* **1992,** *48*, (1), 1-4.
40. Mereiter, K., The crystal structure of Liebigite, $Ca_2UO_2(CO_3)_3\cdot\sim 11H_2O$. *Tschermaks Min. Petr. Mitt.* **1982,** *30*, (4), 277-288.
41. Piret, P.; Piret-Meunier, J.; Declercq, J.-P., Structure of phuralumite. *Acta Crystallographica Section B* **1979,** *35*, (8), 1880-1882.

42. Singer, D. M.; Chatman, S. M.; Rosso, K. M.; Ilton, E. S.; Banfield, J. F.; Waychunas, G. A., U(VI) sorption and reduction kinetics on the magnetite (111) surface. *Environ. Sci. Technol.* **2012,** *submitted*.
43. Skomurski, F. N.; Ilton, E. S.; Engelhard, M. H.; Arey, B. W.; Rosso, K. M., Heterogeneous reduction of U^{6+} by structural Fe^{2+} from theory and experiment. *Geochim. Cosmochim. Acta* **2011,** *75*, 7277-7290.
44. Fuller, C. C.; Bargar, J. R.; Davis, J. A.; Piana, M. J., Mechanisms of uranium interactions with hydroxyapatite: Implications for groundwater remediation. *Environ. Sci. Technol.* **2002,** *36*, (2), 158-165.
45. Chakraborty, S.; Favre, F.; Banerjee, D.; Scheinost, A. C.; Mullet, M.; Ehrhardt, J.-J.; Brendle, J.; Vidal, L. c.; Charlet, L., U(VI) sorption and reduction by Fe(II) sorbed on montmorillonite. *Environ. Sci. Technol.* **2010,** *44*, (10), 3779-3785.
46. Fleet, M., The structure of magnetite. *Acta Crystallographica Section B* **1981,** *37*, (4), 917-920.
47. Wyckoff, R. W. G., *Crystal Structures 1 Second edition*. Interscience Publishers: New York, New York, 1963; p 239-444.
48. Bernier-Latmani, R.; Veeramani, H.; Vecchia, E. D.; Junier, P.; Lezama-Pacheco, J. S.; Suvorova, E. I.; Sharp, J. O.; Wigginton, N. S.; Bargar, J. R., Non-uraninite Products of Microbial U(VI) Reduction. *Environ. Sci. Technol.* **2010,** *44*, (24), 9456-9462.
49. Boyanov, M.; Fletcher, K. E.; Kwon, M. J.; Rui, X.; O'Loughlin, E. J.; Löffler, F. E.; Kemner, K. M., Solution and Microbial Controls on the Formation of Reduced U(IV) Species. *Environ. Sci. Technol.* **2011**, null-null.
50. Bargar, J. R.; Reitmeyer, R.; Davis, J. A., Spectroscopic confirmation of uranium(VI)-carbonato adsorption complexes on hematite. *Environ. Sci. Technol.* **1999,** *33*, (14), 2481-2484.
51. Bargar, J. R.; Reitmeyer, R.; Lenhart, J. J.; Davis, J. A., Characterization of U(VI)-carbonato ternary complexes on hematite: EXAFS and electrophoretic mobility measurements. *Geochim. Cosmochim. Acta* **2000,** *64*, (16), 2737-2749.
52. Catalano, J. G.; Brown Jr., G. E., Uranyl adsorption onto montmorillonite: Evaluation of binding sites and carbonate complexation. *Geochim. Cosmochim. Acta* **2005,** *69*, (12), 2995-3005.
53. Sylwester, E. R.; Hudson, E. A.; Allen, P. G., The structure of uranium(VI) sorption complexes on silica, alumina, and montmorillonite. *Geochim. Cosmochim. Acta* **2000,** *64*, (14), 2431-2438.
54. Muñoz, M.; Argoul, P.; Farges, F., Continuous Cauchy wavelet transform analyses of EXAFS spectra: A qualitative approach. *Am. Mineral.* **2003,** *88*, 694-700.
55. Kelly, S. D.; Kemner, K. M.; Brooks, S. C., X-ray absorption spectroscopy identifies calcium-uranyl-carbonate complexes at environmental concentrations. *Geochim. Cosmochim. Acta* **2007,** *71*, (4), 821-834.
56. Bernhard, G.; Geipel, G.; Reich, T.; Brendler, V.; Amayri, S.; Nitsche, H., Uranyl(VI) carbonate complex formation: Validation of the $Ca_2UO_2(CO_3)_3$(aq.) species. *Radiochim. Acta* **2001,** *89*, (8), 511-518.
57. Amayri, S.; Reich, T.; Arnold, T.; Geipel, G.; Bernhard, G., Spectroscopic characterization of alkaline earth uranyl carbonates. *J. Solid State Chem.* **2005,** *178*, (2), 567-577.
58. Gorman-Lewis, D.; Elias, P. E.; Fein, J. B., Adsorption of aqueous uranyl complexes onto *Bacillus subtilis* cells. *Environ. Sci. Technol.* **2005,** *39*, (13), 4906-4912.
59. Sheng, L.; Szymanowski, J.; Fein, J. B., The effects of uranium speciation on the rate of U(VI) reduction by *Shewanella oneidensis* MR-1. *Geochim. Cosmochim. Acta* **2011,** *75*, (12), 3558-3567.
60. Skomurski, F. N.; Kerisit, S.; Rosso, K. M., Structure, charge distribution, and electron hopping dynamics in magnetite (Fe_3O_4) (1 0 0) surfaces from first principles. *Geochim. Cosmochim. Acta* **2010,** *74*, (15), 4234-4248.
61. Fox, P. M.; Davis, J. A.; Zachara, J. M., The effect of calcium on aqueous uranium(VI) speciation and adsorption to ferrihydrite and quartz. *Geochim. Cosmochim. Acta* **2006,** *70*, (6), 1379-1387.
62. Wu, W. M.; Carley, J.; Fienen, M.; Mehlhorn, T.; Lowe, K.; Nyman, J.; Luo, J.; Gentile, M. E.;

Rajan, R.; Wagner, D.; Hickey, R. F.; Gu, B. H.; Watson, D.; Cirpka, O. A.; Kitanidis, P. K.; Jardine, P. M.; Criddle, C. S., Pilot-scale in situ bioremediation of uranium in a highly contaminated aquifer. 1. Conditioning of a treatment zone. *Environ. Sci. Technol.* **2006,** *40*, (12), 3978-3985.
63. Guillaumont, R.; Fanghänel, T.; Fuger, J.; Grenthe, I.; Neck, V.; Palmer, D. A.; Rand, M. H., *Update on the Chemical Thermodynamics of Uranium, Neptunium, Plutonium, Americium and Technetium*. Elsevier: Amsterdam, 2003; Vol. 5.
64. Wander, M. C. F.; Kerisit, S.; Rosso, K. M.; Schoonen, M. A. A., Kinetics of triscarbonato uranyl reduction by aqueous ferrous iron: A theoretical study. *J. Phys. Chem. A* **2006,** *110*, (31), 9691-9701.

DISCLAIMER